ACS APPLIED MATERIALS & INTERFACES

RESEARCH ARTICLE

www.acsami.org

Interconnected MoO_2 Nanocrystals with Carbon Nanocoating as High-Capacity Anode Materials for Lithium-ion Batteries

Liang Zhou,[†,‡] Hao Bin Wu,[†,‡] Zhiyu Wang,[†] and Xiong Wen (David) Lou*[,†,‡]

[†]School of Chemical and Biomedical Engineering, Nanyang Technological University, 70 Nanyang Drive, Singapore 637457

[‡]Energy Research Institute @ NTU, Nanyang Technological University, 50 Nanyang Drive, Singapore 637553 (Singapore)

Supporting Information

ABSTRACT: A facile one-pot hydrothermal method has been developed for the preparation of carbon-coated MoO_2 nanocrystals. The annealed MoO_2−C nanocomposite consists of interconnected MoO_2@C nanocrystals. When evaluated for lithium storage capabilities, these MoO_2@C nanocrystals exhibit high specific capacities (~ 640 mA h g^{-1} at 200 mA g^{-1} and ~575 mA h g^{-1} at 400 mA g^{-1}) and excellent cycling stability. In view of the excellent lithium storage properties and the ease in large-scale preparation, the as-synthesized MoO_2−C nanocomposite might be used as promising anode materials for high-performance lithium-ion batteries.

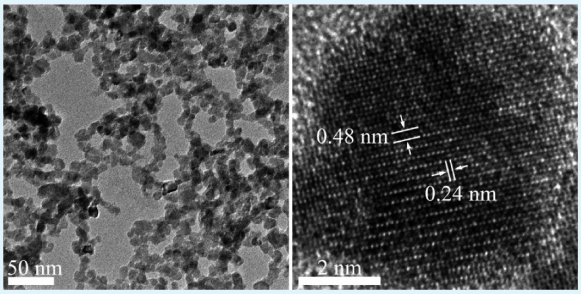

KEYWORDS: anode, lithium-ion battery, MoO_2, nanocomposite, carbon coating

1. INTRODUCTION

Molybdenum oxides (MoO_x, $2 \le x \le 3$) have attracted much attention as host materials for lithium storage because of their rich chemistry associated with multiple valence states, low electrical resistivity, high electrochemical activity toward lithium, and affordable cost.[1−10] In particular, molybdenum dioxide (MoO_2) with a disordered rutile structure possesses metallic conductivity and high theoretical capacity (838 mA h g^{-1}). However, it is known that MoO_2 undergoes significant volume change during lithiation and delithiation, which leads to breakdown of electrical pathways (the so-call pulverization) and thereafter rapid capacity fading. In addition, the lithiation of bulk MoO_2 is limited to addition-type reaction with only one-electron reduction ($xLi + MoO_2 = Li_xMoO_2$, $0 \le x \le 0.98$) at room temperature because of the sluggish kinetics, although the consecutive conversion reaction with another three-electron reduction ($Li_{0.98}MoO_2 + 3.02Li = 2Li_2O + Mo$) is thermodynamically feasible.[11] Thus, bulk MoO_2 featured by low specific capacity and poor cycling stability is not suitable as a host material for lithium storage.

In a manner similar to other rutile structured metal oxides such as TiO_2,[12] SnO_2,[13] and MnO_2,[14−16] the electroactivity of nanostructured MoO_2 is significantly enhanced compared to its bulk counterpart due to the large surface area and short dimensions for charge diffusion.[17−20] For example, tremella-like MoO_2 consisting of ultrathin nanosheets,[18] ordered mesoporous MoO_2,[19] and hierarchically nanostructured MoO_2 monolith[20] are shown to deliver high reversible specific capacities of 600−750 mA h g^{-1}. Despite the high specific capacity and mitigated pulverization problem, the cycling stability of most pure MoO_2 nanostructures is still not satisfactory. On the other hand, hybridizing nanostructured MoO_2 with conductive and elastic carbon is an effective strategy to improve the structural integrity, hence the cycling performance.[21−27] In this regard, MoO_2−carbon hybrid nanowires,[23] carbon-coated MoO_2 nanospheres and nanofibers,[24,25] and MoO_2−graphene nanocomposites[26] have been reported recently, and these MoO_2−C hybrids do outperform bare MoO_2 in cycling. Considering that the number of MoO_2−C nanostructures reported is still quite limited up to now, the synthesis of novel nanostructured MoO_2−C nanocomposites for lithium storage is highly desired.

Herein, we report a one-pot hydrothermal synthesis of MoO_2−C nanocomposites composed of interconnected MoO_2 nanocrystals with carbon nanocoating on the surface. When evaluated as an anode material for lithium-ion batteries, the annealed MoO_2−C nanocomposite exhibits high reversible specific capacities (~640 mA h g^{-1} at 200 mA g^{-1} and ~575 mA h g^{-1} at 400 mA g^{-1}) and excellent cycling stability.

2. EXPERIMENTAL SECTION

Materials Synthesis. In a typical synthesis, 10 mmol of Mo powder was dissolved in 40 mL of 15 wt % H_2O_2 to form an orange-colored clear solution. Afterward, 20 mL of ethylene glycol was added into the above solution. The solution was then transferred into a Teflon-lined stainless-steel autoclave, which was then sealed and hydrothermally treated at 200 °C for 24 h. The black products (designated as as-made MoO_2−C) were collected by centrifugation, rinsed with water and ethanol for three times, and dried at 60 °C. The as-made MoO_2−C was further annealed at 500 °C for 5 h in nitrogen flow to obtain the final product (designated as annealed MoO_2−C).

Received: October 2, 2011
Accepted: November 11, 2011
Published: November 11, 2011

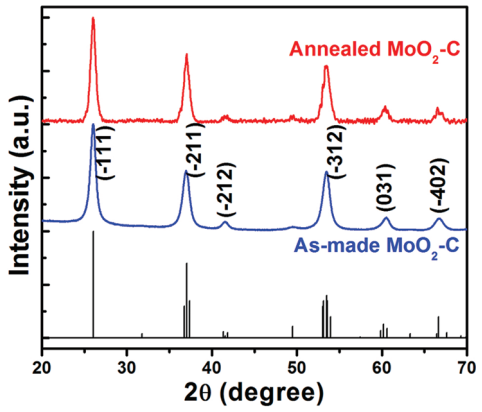

Figure 1. XRD patterns of the as-made and annealed MoO_2−C nanocomposites.

Characterization. X-ray diffraction (XRD) measurements were performed on a Bruker D8 Advanced X-ray Diffractometer with Ni filtered Cu Kα radiation. Field emission scanning electron microscopy (FESEM) images were obtained on a JEOL JSM 6700F microscope. Transmission electron microscopy (TEM) images were taken on a JEOL 2010 microscope. Thermogravimetric analysis (TGA) was carried out under air flow with a temperature ramp of 5 °C min^{-1}. Nitrogen adsorption−desorption isotherms were measured at −196 °C on a nitrogen sorption apparatus (Autosorb 6B, Quantachrome).

Electrochemical Measurement. The electrochemical measurements were carried out in two-electrode Swagelok-type cells. The working electrodes consisted of 70% MoO_2−C nanocomposites, 20% carbon black (Super−P-Li), and 10% polyvinylidene fluoride (PVDF). Metallic lithium was used as both the counter electrode and reference electrode. 1 M $LiPF_6$ in a mixture of ethylene carbonate and diethyl carbonate (1/1 by weight) was used as the electrolyte. Cell assembly was carried out in an Ar-filled glovebox with moisture and oxygen concentration strictly controlled. Cyclic voltammetry (0.01−3.0 V, 0.2 mV s^{-1}) and electrochemical impedance measurements were performed on a CHI660C electrochemical workstation. The galvanostatic charge−discharge tests were performed on a NEWARE battery tester at current densities of 200 and 400 mA g^{-1} in the voltage range of 0.1−3.0 V vs Li/Li^+.

3. RESULTS AND DISCUSSION

The MoO_2−C nanocomposites are prepared by hydrothermal treatment of peroxo-molybdic acid aqueous solution in the presence of ethylene glycol, which acts as both the reducing agent and the carbon source.

XRD is first employed to characterize the crystalline structure and crystallinity of the as-made and annealed MoO_2−C nanocomposites, and the results are shown in Figure 1. The XRD patterns of both samples can be assigned to the pure monoclinic MoO_2 phase (JCPDS Card No.: 32−0671, space group: $P2_1/n$, a = 5.606 Å, b = 4.859 Å, c = 5.537 Å, $\alpha = \gamma = 90°$, β = 119.37°) with a disordered rutile structure. The significantly broadened diffraction peaks of the as-made MoO_2−C indicate its nanocrystalline characteristic. Interestingly, no significant sharpening of the diffraction peaks can be observed after annealing, which suggests that crystal growth during annealing has been effectively suppressed by the existence of carbon layer on the nanocrystals.

SEM and TEM are further employed to characterize the morphology and detailed structure of the products. As can be seen from the SEM image (Figure 2a), the as-made MoO_2−C is composed of loosely aggregated nanocrystals with sizes around 10 nm. From the TEM image (Figure 2b), it can be clearly observed that the as-made MoO_2−C nanocrystals are interconnected with each other. This interesting structure provides good physical contact between the nanocrystals and is beneficial for electron conduction. As expected, the selected area electron diffraction (SAED) pattern (Figure 2c) of the as-made MoO_2−C nanocrystals shows a set of concentric rings, indicating the polycrystalline nature of the sample. The diffraction rings from inside to outside can be indexed to the (−111), (−211), (−212), (−312), (031), and (−402) planes of monoclinic MoO_2, respectively. Two sets of lattice fringes, corresponding to the (−101) (0.48 nm) and (111) (0.24 nm) interplane spacings, can be clearly distinguished from the high-resolution TEM (HRTEM) image of the as-made MoO_2−C nanocomposite.

After being annealed at 500 °C in nitrogen flow, the annealed MoO_2−C nanocrystals are packed more densely as can be observed from the SEM (Figure 2e) and TEM images (Figure 2f). Similar to the as-made MoO_2−C nanocomposites, the (−111), (−211), (−212), (−312), (031), and (−402) diffraction rings can be clearly observed in the SAED pattern of the annealed sample (Figure 2g). From the TEM image with a relatively high magnification (Figure 2h), a thin amorphous carbon layer with a thickness of ∼4 nm can be clearly observed on the surface of the tiny nanocrystals.

N_2 adsorption−desorption is conducted to examine the textural properties of the as-made and annealed MoO_2−C nanocomposites. The N_2 adsorption−desorption isotherms and the corresponding Barrett−Joyner−Halenda (BJH) pore size distributions are shown in Figure 3a and 3b, respectively. Both samples exhibit type IV isotherms with H2 type hysteresis loops, indicating the presence of mesoporous structures. The as-made MoO_2−C nanocomposite has a large Brunauer−Emmett−Teller (BET) surface area of 84.9 m^2 g^{-1}, a high total pore volume of 0.22 cm^3 g^{-1}, and a relatively broad pore size distribution in the range of 5 − 30 nm. After annealing, the sample shows similar pore size distribution, but a smaller BET surface area (27.5 m^2 g^{-1}) and a lower total pore volume (0.08 cm^3 g^{-1}). This result agrees well with the SEM and TEM observations, that is, the annealed MoO_2−C nanocrystals pack more densely than the as-made sample and the interconnection between the nanocrystals is greatly strengthened.

Next, TGA is employed to quantitatively determine the carbon content in the annealed MoO_2−C nanocomposite. As can be seen from Figure S1, the TGA curve is relatively complicated because of the combustion of carbon and the oxidation of MoO_2 at the same time. The weight loss (∼ 8.0 wt %) below 200 °C is likely due to the loss of adsorbed moisture; while the weight change (∼ 5.4 wt %) in the range of 200 − 600 °C is due to the simultaneous oxidation of MoO_2 and combustion of carbon. The weight retention at 600 °C is 86.6 wt %. Assuming that MoO_2 is thoroughly oxidized to MoO_3, the MoO_2 and carbon contents in the composite can be estimated to be 77.0 and 15.0% by weight, respectively.

To understand the lithium storage properties of the MoO_2−C nanocomposites, cyclic voltammetry and galvanostatic charge−discharge measurements have been performed. Figure 4 displays the initial three consecutive cyclic voltammograms (CVs) of the MoO_2−C electrode. There is a substantial variation in the CVs of the first and subsequent cycles. A pronounced reduction peak (lithium insertion) is observed at 0.94 V in the

first cathodic polarization process. It may be attributed to the phase transition from the orthorhombic phase to the monoclinic phase upon lithium insertion as suggested by Dahn and McKinnon.[2] The absence of solid electrolyte interphase (SEI) film peak in the first cathodic sweep is consistent with Ku et al. and Wang et al.'s reports,[11,24] whereas it is in contrast to Sun et al. and Luo et al.'s reports.[20,25,26] This discrepancy may result from the different surface properties of the electrode materials. In the following anodic polarization, two overlapping oxidation peaks (lithium extraction), which can be ascribed to the phase transitions (monoclinic-orthorhombic-monoclinic) in partially lithiated Li_xMoO_2 ($0 \le x \le 0.98$),[2,19] are observed at 1.5−2.0 V. These two phase transitions are highly reversible in the subsequent lithium insertion/extraction cycles as indicated by the pronounced two pairs of reduction/oxidation peaks (1.52/1.76 V and 1.20/1.56 V).

Figure 5a displays representative galvanostatic discharge−charge curves of the annealed MoO_2−C electrode at a current density of 200 mA g^{-1} in the voltage range of 0.1−3.0 V vs Li/Li^+. The annealed MoO_2−C electrode delivers initial discharge/charge capacities of 1040 and 543 mA h g^{-1}, respectively, with a Coulombic efficiency of 52.2%. The charge capacity increases upon cycling and reaches ~620 mA h g^{-1} after 10 cycles, while the discharge capacity does not vary much since the second cycle. Thus, the Coulombic efficiency increases rapidly and stabilizes at ~95% after several cycles (see the Supporting Information, Figure S2). The cycling performance of the as-made and annealed MoO_2−C electrodes at current densities of 200 and 400 mA g^{-1} is shown in Figure 5b. From the second cycle onward, the annealed MoO_2−C exhibits very stable cycling performance up to 50 cycles. After 50 cycles at 200 mA g^{-1}, a high discharge capacity of 629 mA h g^{-1} can be retained, corresponding to 98% of the discharge capacity for the second cycle (642 mA h g^{-1}). Even at a relatively high current density of 400 mA g^{-1}, a capacity of 554 mA h g^{-1} can be retained after 50 cycles. The capacity begins to decrease after 50 cycles, probably due to the detachment of active material from the current collector. Nevertheless, the cycling stability is superior to most previous reports, in which cycling performance for only 20−30

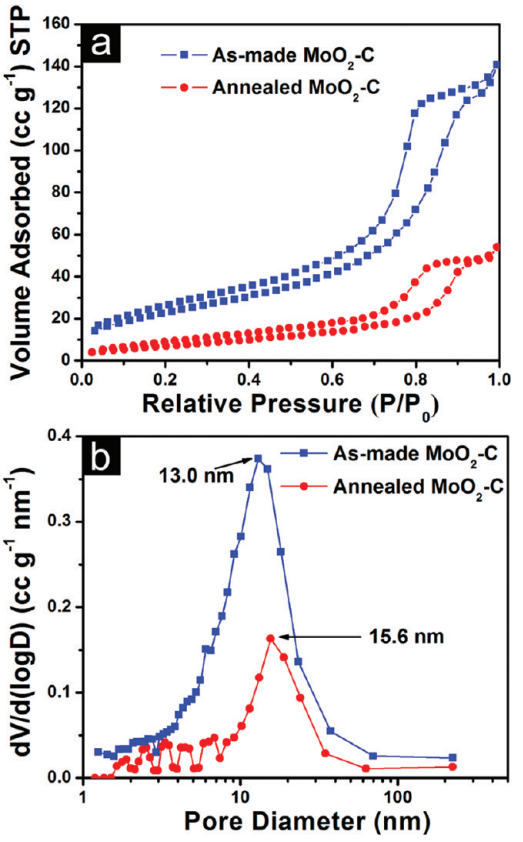

Figure 3. (a) N_2 adsorption−desorption isotherms ands (b) BJH pore size distributionof the as-made and annealed MoO_2−C nanocomposites.

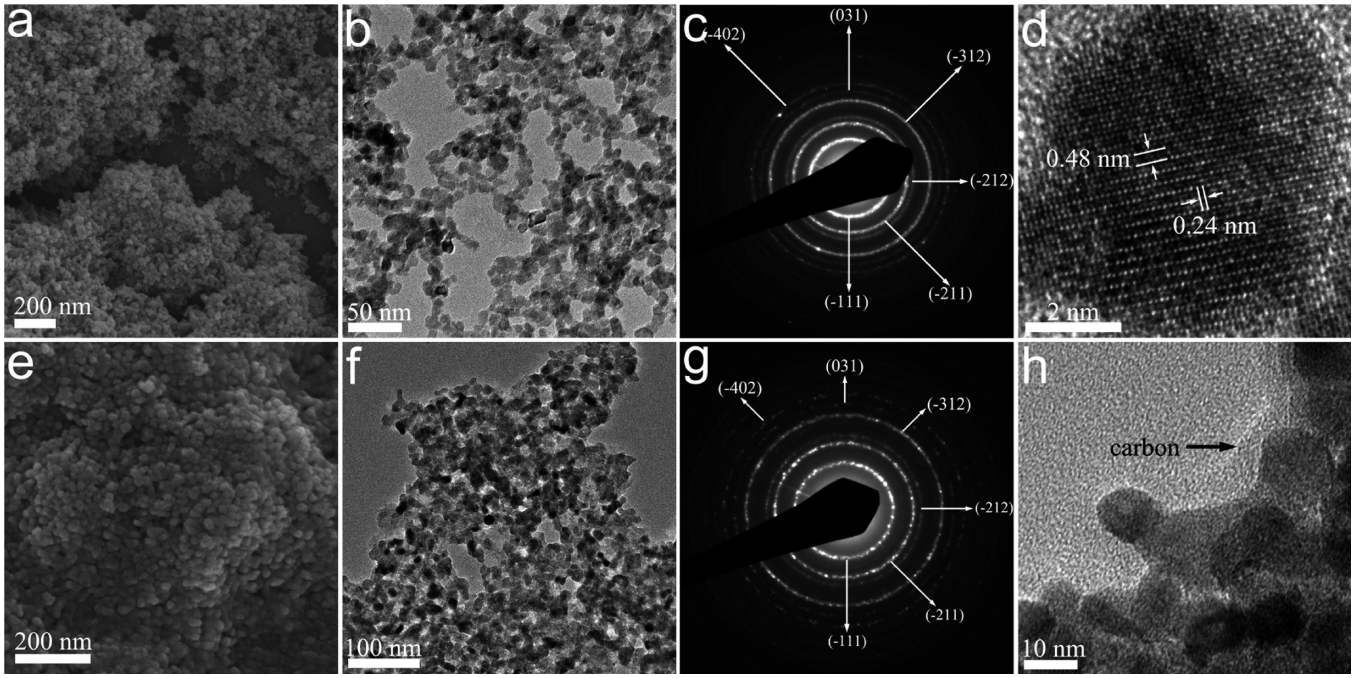

Figure 2. SEM, TEM, SAED patterns, and HRTEM images of the (a−d) as-made and (e−h) annealed MoO_2−C nanocomposites.

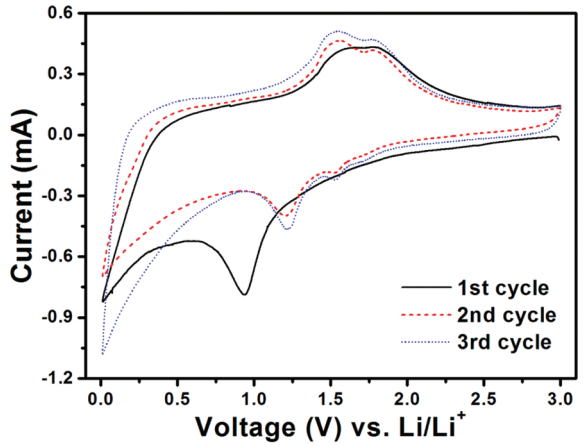

Figure 4. First three consecutive CVs of the annealed MoO_2−C electrode at a scan rate of 0.2 mV s^{-1} in the voltage range of 0.01−3.0 V vs Li/Li^+.

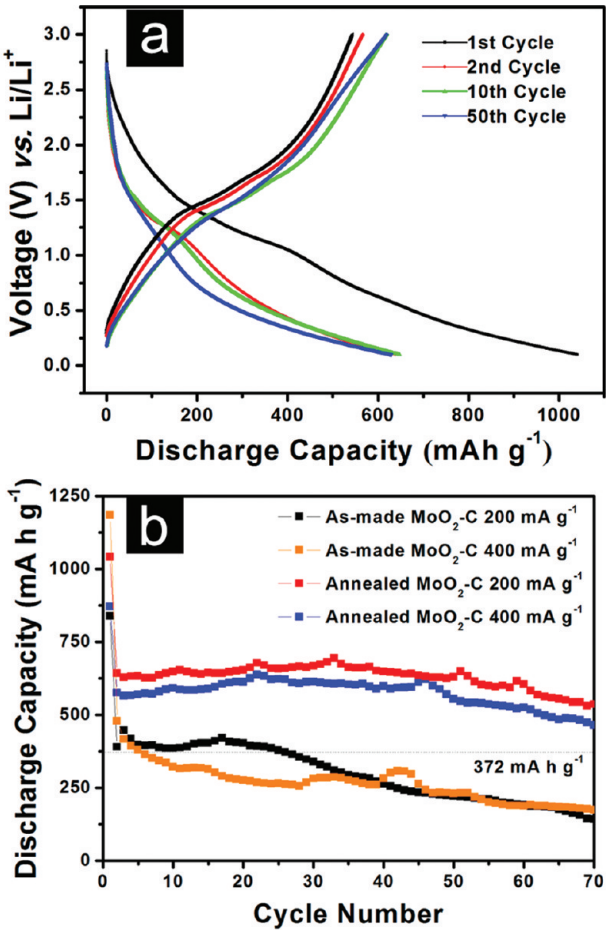

Figure 5. (a) Representative galvanostatic discharge−charge curves of the annealed MoO_2−C electrode at a current density of 200 mA g^{-1} in the voltage range of 0.1 − 3.0 V vs Li/Li^+. (b) Cycling performance of the as-made and annealed MoO_2−C electrodes at current densities of 200 and 400 mA g^{-1} in the voltage range of 0.1−3.0 V vs Li/Li^+.

cycles were provided.[11,17−24] In contrast to the annealed MoO_2−C, the as-made MoO_2−C exhibits a low discharge capacity and rapid fading of reversible capacity. The inferior electrochemical performance of the as-made MoO_2−C may be attributed to the incomplete carbonization of the organic species on the surface, which might absorb lots of moisture and hence deteriorate the conductivity (see Figure S3 in the Supporting Information).

The excellent lithium storage performance of the annealed MoO_2−C nanocomposite could be attributed to the following factors: (1) The highly accessible large surface and large amount of defect sites of the MoO_2−C nanocomposite render the conversion type reaction ($Li_{0.98}MoO_2$ + 3.02Li = $2Li_2O$ + Mo) kinetically feasible, therefore leading to a large lithium storage capacity. (2) The dimension for Li^+ diffusion is significantly reduced to ∼5 nm (half of the diameter of the MoO_2−C nanocrystals), thus the rate capability is improved when compared to MoO_2 structures with a larger size. (3) The interconnected MoO_2−C framework with good conductivity not only provides the electron conduction pathway but also reduces the internal resistance of the cells. (4) The elastic carbon layer over the MoO_2 nanocrystals not only buffers the stress caused by the drastic volume change but also prevents the aggregation of the nanoparticles and pulverization of the electrode material upon cycling, hence improving the structural integrity and cycling stability.

4. CONCLUSION

In summary, a MoO_2−C nanocomposite composed of interconnected MoO_2 nanocrystals with carbon nanocoating on the surface has been successfully synthesized by a facile one-pot hydrothermal method followed by thermal annealing in nitrogen flow. When evaluated as an anode material for lithium-ion batteries, the annealed MoO_2−C nanocomposite exhibits high specific capacity and excellent cycling stability. For example, a high discharge capacity of 629 mA h g^{-1} can be retained when cycled at 200 mA g^{-1} for 50 cycles. The excellent lithium storage properties and the great simplicity in large-scale synthesis might make such a MoO_2−C nanocomposite promising as an anode material for high-performance lithium-ion batteries.

■ ASSOCIATED CONTENT

Supporting Information. TGA curve, Coulombic efficiency, and Nyquist plots. This material is available free of charge via the Internet at http://pubs.acs.org/.

■ AUTHOR INFORMATION

Corresponding Author
*E-mail: xwlou@ntu.edu.sg.

■ REFERENCES

(1) Auborn, J. J.; Barberio, Y. L. *J. Electrochem. Soc.* **1987**, *134*, 638.
(2) Dahn, J. R.; McKinnon, W. R. *Solid State Ionics* **1987**, *23*, 1.
(3) Manthiram, A.; Tsang, C. *J. Electrochem. Soc.* **1996**, *143*, L143.
(4) Dampier, F. W. *J. Electrochem. Soc.* **1974**, *121*, 656.
(5) Whittingham, M. S. *J. Electrochem. Soc.* **1976**, *123*, 315.
(6) Lee, S. H.; Kim, Y. H.; Deshpande, R.; Parilla, P. A.; Whitney, E.; Gillaspie, D. T.; Jones, K. M.; Mahan, A. H.; Zhang, S. B.; Dillon, A. C. *Adv. Mater.* **2008**, *20*, 3627.
(7) Mai, L. Q.; Hu, B.; Chen, W.; Qi, Y. Y.; Lao, C. S.; Yang, R. S.; Dai, Y.; Wang, Z. L. *Adv. Mater.* **2007**, *19*, 3712.
(8) Li, W. Y.; Cheng, F. Y.; Tao, Z. L.; Chen, J. *J. Phys. Chem. B* **2006**, *110*, 119.

(9) Chen, J. S.; Cheah, Y. L.; Madhavi, S.; Lou, X. W. *J. Phys. Chem. C* **2010**, *114*, 8675.
(10) Zhou, L.; Yang, L. C.; Yuan, P.; Zou, J.; Wu, Y. P.; Yu, C. Z. *J. Phys. Chem. C* **2010**, *114*, 21868.
(11) Ku, J. H.; Jung, Y. S.; Lee, K. T.; Kim, C. H.; Oh, S. M. *J. Electrochem. Soc.* **2009**, *156*, A688.
(12) Hu, Y. S.; Kienle, L.; Guo, Y. G.; Maier, J. *Adv. Mater.* **2006**, *18*, 1421.
(13) Lou, X. W.; Wang, Y.; Yuan, C. L.; Lee, J. Y.; Archer, L. A. *Adv. Mater.* **2006**, *18*, 2325.
(14) Ren, Y.; Armstrong, A. R.; Jiao, F.; Bruce, P. G. *J. Am. Chem. Soc.* **2010**, *132*, 996.
(15) Luo, J. Y.; Zhang, J. J.; Xia, Y. Y. *Chem. Mater.* **2006**, *18*, 5618.
(16) Jiao, F.; Bruce, P. G. *Adv. Mater.* **2007**, *19*, 657.
(17) Liang, Y. G.; Yang, S. J.; Yi, Z. H.; Sun, J. T.; Zhou, Y. H. *Mater. Chem. Phys.* **2005**, *93*, 395.
(18) Yang, L. C.; Gao, Q. S.; Zhang, Y. H.; Tang, Y.; Wu, Y. P. *Electrochem. Commun.* **2008**, *10*, 118.
(19) Shi, Y. F.; Guo, B. K.; Corr, S. A.; Shi, Q. H.; Hu, Y. S.; Heier, K. R.; Chen, L. Q.; Seshadri, R.; Stucky, G. D. *Nano Lett.* **2009**, *9*, 4215.
(20) Sun, Y. M.; Hu, X. L.; Yu, J. C.; Li, Q.; Luo, W.; Yuan, L. X.; Zhang, W. X.; Huang, Y. H. *Energy Environ. Sci.* **2011**, *4*, 2870.
(21) Ji, X. L.; Herle, S.; Rho, Y. H.; Nazar, L. F. *Chem. Mater.* **2007**, *19*, 374.
(22) Yang, L. C.; Gao, Q. S.; Tang, Y.; Wu, Y. P.; Holze, R. *J. Power Sources* **2008**, *179*, 357.
(23) Gao, Q. S.; Yang, L. C.; Lu, X. C.; Mao, J. J.; Zhang, Y. H.; Wu, Y. P.; Tang, Y. *J. Mater. Chem.* **2010**, *20*, 2807.
(24) Wang, Z. Y.; Chen, J. S.; Zhu, T.; Madhavi, S.; Lou, X. W. *Chem. Commun.* **2010**, *46*, 6906.
(25) Luo, W.; Hu, X. L.; Sun, Y. M.; Huang, Y. H. *Phys. Chem. Chem. Phys.* **2011**, *13*, 16735.
(26) Sun, Y. M.; Hu, X. L.; Luo, W.; Huang, Y. H. *ACS Nano* **2011**, *5*, 7100.
(27) Yoon, S.; Manthiram, A. *J. Mater. Chem.* **2011**, *21*, 4082.